Numerical modeling of rock fracturing under uniaxial compression based on four-dimensional lattice spring model

Yimin Hao*, Yiming Li, Fuxin Rui

State Key Laboratory of Hydraulic Engineering Simulation and Safety, School of Civil Engineering, Tianjin University

Tianjin, China

* yimin_hao@tju.edu.cn

***Abstract*—Four-dimensional lattice spring model (4D-LSM) is a discrete numerical method suitable for calculating the mechanical response of solids based on the spatial extra dimension theory in modern physics. In this work, the parameters of numerical model are calibrated according to uniaxial compression tests of three rock samples. The results show that the uniaxial compressive strength and failure modes are almost consistent with the experimental results. The fracture patterns of other cracked specimens in uniaxial compression tests are predicted. We conclude that 4D-LSM is a powerful tool for studying the mechanical behavior, strength and failure of rocks.**

Keywords—Four-dimensional lattice spring model, rock fracturing, calibration, numerical prediction

I Numerical methods and software

The four-dimensional lattice spring model (4D-LSM) (Zhao, 2017) is developed based on the three-dimensional discrete spring element method (DLSM). In DLSM, the model is composed of discrete spherical particles connected by a normal spring and a tangential spring. It is solved by an explicit central finite difference scheme. Compared with the traditional discrete method, DLSM does not require macro-parameter calibration. And the degree of freedom is half of the discrete element method (DEM). The model of 4D-LSM in visual 3D space and its mapped model in parallel world are closely connected through the 4D interactions (Hu, 2018). And there are three types of 4D interactions for a cubic lattice model, which are represented by k_α, k_β and k_γ (see Fig. 1(b)). The calculation cycle is illustrated in Fig. 1(a). Given the particle displacements (either prescribed initially or obtained from the previous time step), new contacts and broken bonds are detected. The list of neighboring particles for each particle is updated. Then, contact and spring forces between particles are calculated according to the prescribed force-displacement relations.

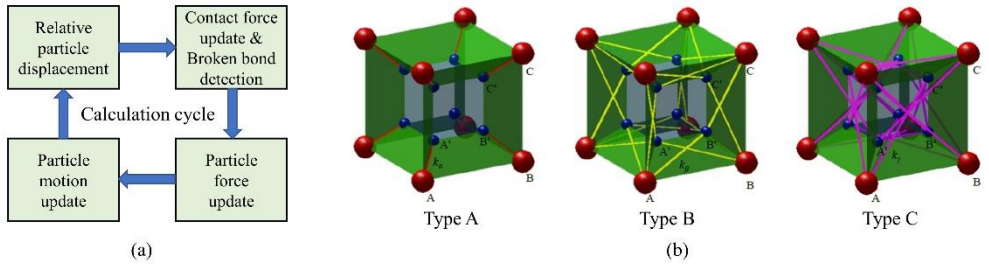

Fig. 1. The four-dimensional lattice spring model: (a) Calculation cycle; (b) Three types of 4D interactions.

The force and normal vector of each particle has three components in DLSM, whereas, the components of force and normal vector increase to four in 4D-LSM. It is worth noting that the springs representing the interactions between particles in the original 3D model all use the same spring stiffness (k^{3D}), while the springs representing the fourth interactions use different stiffness and the above three types of stiffness can be described with 4D stiffness ratio (λ^{4D}). Through theoretical derivation, Zhao (Zhao, 2017) proposed a formula for determining 4D spring stiffness to represent the isotropic elasticity, which can be expressed as:

$$k_\alpha = k_\beta = 4/3 k_\gamma = \lambda^{4D} k^{3D} \tag{1}$$

In 4D-LSM, the interaction force between particles obeys Newton's second law, and there is only a normal force without shearing. The mathematical expression is:

$$\boldsymbol{F}_{ij} = k u_n \mathbf{n}_{ij} \tag{2}$$

where $\boldsymbol{F}_{ij}$ is the force from particle i to particle j, k is the stiffness of the spring, $\mathbf{n}_{ij}$ is the normal vector from particle i to particle j and u_n is the deformation of the spring. The spring deformation u_n and spring normal $\mathbf{n}_{ij}$ can be calculated with the following expression:

$$u_n = \left|\mathbf{x_j} - \mathbf{x_i}\right| - \left|\mathbf{x_j^0} - \mathbf{x_i^0}\right| \tag{3}$$

$$\mathrm{n}_{ij} = \frac{\mathbf{x}_j - \mathbf{x}_j}{\left|\mathbf{x}_j - \mathbf{x}_j\right|} \tag{4}$$

where x is the current position of the mass point, x0 is the corresponding initial position, and |·| refers to get the norm of a vector.

For elastic problems, there are only two parameters, i.e. k^{3D} and λ^{4D}, are needed in 4D-LSM, and these mesoscopic elastic parameters can be calculated by macroscopic elastic parameters, i.e. E and ν, through the following equations (Zhao, 2017):

$$k^{3D} = \frac{6V^{3D}E}{\sum l_{3D,i}^2} \tag{5}$$

$$\lambda^{4D} = -211.13493779v^3 + 162.84655851v^2 - 55.42449719v + 6.92902211 \tag{6}$$

where k^{3D} is the stiffness of spring, λ^{4D} is the volume of the 3D model, $l_{3D,i}$ is the length of the 3D springs, E is the elastic modulus and ν is the Poisson's ratio. More details on the derivation and validation of 4D-LSM are suggested to be found in the work of Zhao (2017). In this paper, 4D-LSM will be used for modeling and research.

Stage I

II-1 Numerical modelling

As shown in the Fig. 2, the dimensions of numerical model are 50 mm × 50 mm × 30 mm and the particle size is 0.5 mm. The total number of particles is 600,000. The upper and lower boundaries of the model are wall boundaries. A uniform downward force of F_y is applied on the upper part of the model with a speed of 1 mm/min until the model is damaged. The model adopts multi-body failure criterion and adaptive damping. The rock mass is assumed to be isotropic and homogeneous.

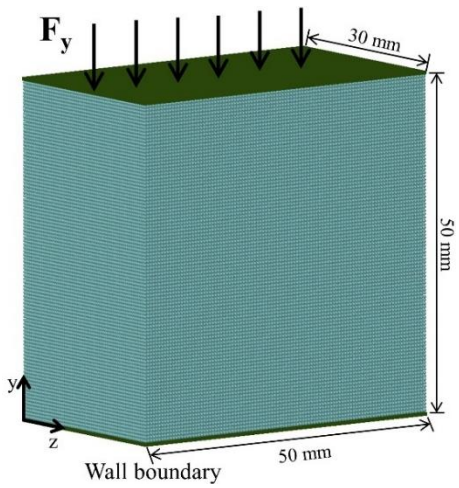

Fig. 2. Numerical model.

III-1 Calibration results

3.1 Granite (sample 1)

According to the uniaxial compression test results of granite, the model is calibrated with E_{50}. As shown in Fig. 3(a), the red curve is the experimental result and the blue curve is the numerical simulation result after parameter calibration. Six characteristic points (A, B, C, D, E and F) of the curve are selected to describe the failure process of the sample. It can be found from the figure that the uniaxial compressive strength of the model is 265.50 kN and the experimental result is 277.48 kN, with a difference of 4.32%. The failure process of the model is shown in Fig. 3(b). The calibration results of granite parameters are shown in Table 1.

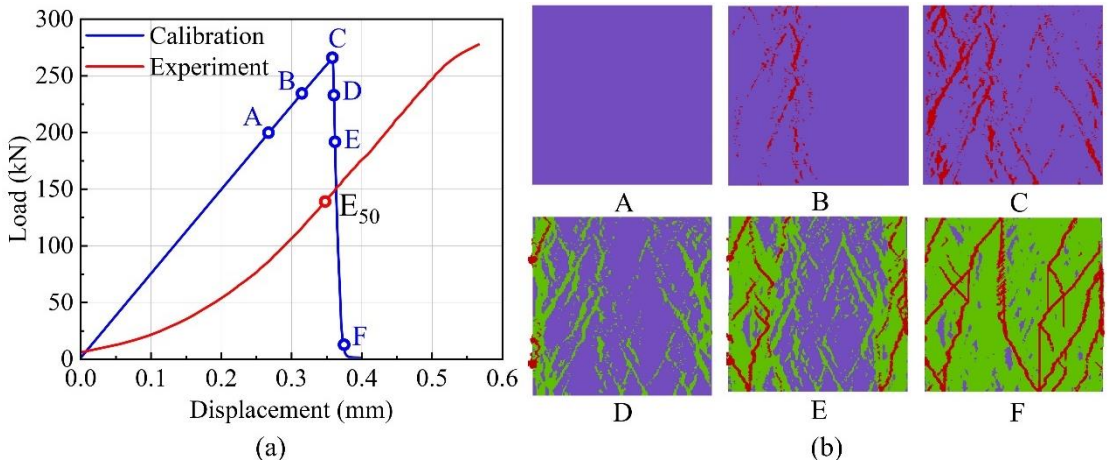

Fig. 3. Numerical simulation of uniaxial compressive strength test of granite: (a) uniaxial compressive strength curve; (b) rock fracturing process in six stages

Table 1. Calibration results of granite parameters

Parameters	Elastic modulus (GPa)	Poisson's ratio	Density (g/cm^3)	Tensile strength (MPa)	Cohesion (MPa)	Friction angle (°)
Granite	25	0.22	2.63	16	34	50

3.2 Marble (sample 1)

According to the uniaxial compression test results of granite, the model is calibrated with E_{50}. As shown in Fig. 4(a), the red curve is the experimental result and the blue curve is the numerical simulation result after parameter calibration. Six characteristic points (A, B, C, D, E and F) of the curve are selected to describe the failure process of the sample. It can be found from the figure that the uniaxial compressive strength of the model is 214.15 kN and the experimental result is 224.88 kN, with a difference of 4.77%. The failure process of the model is shown in Fig. 4(b). The calibration results of granite parameters are shown in Table 2.

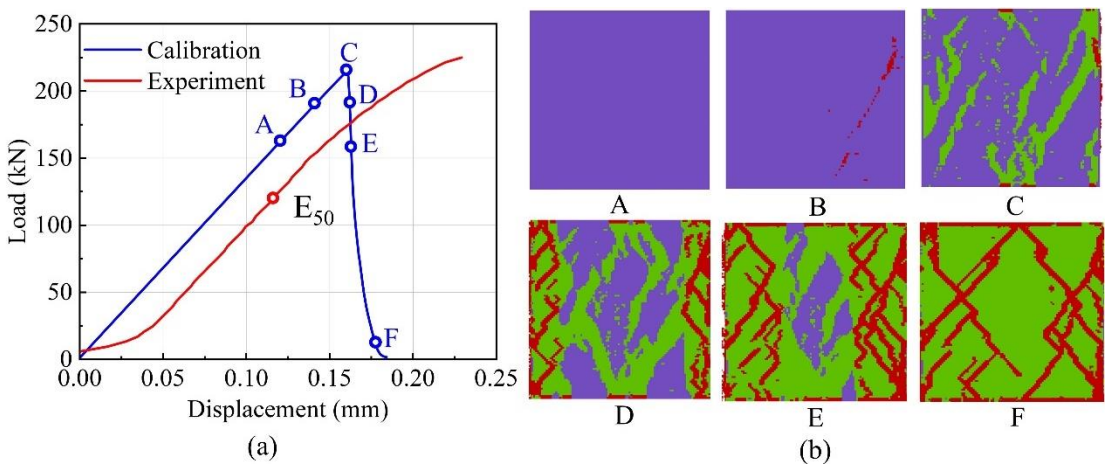

Fig. 4. Uniaxial compressive strength curve of marble: (a) uniaxial compressive strength curve; (b) rock fracturing process in six stages

Table 2. Numerical model parameters of marble

Parameters	Elastic modulus (GPa)	Poisson's ratio	Density (g/cm^3)	Tensile strength (MPa)	Cohesion (MPa)	Friction angle (°)
Marble	45	0.24	2.85	12	27	51

3.3 Red-sandstone (sample 1)

According to the uniaxial compression test results of granite, the model is calibrated with E_{50}. As shown in Fig. 5(a), the red curve is the experimental result and the blue curve is the numerical simulation result after parameter calibration. Six characteristic points (A, B, C, D, E and F) of the curve are selected to describe the failure process of the sample. It can be found from the figure that the uniaxial compressive strength of the model is 183.87 kN and the experimental result is 189.89 kN, with a difference of 3.17%. The failure process of the model is shown in Fig. 5(b). The calibration results of granite parameters are shown in Table 3.

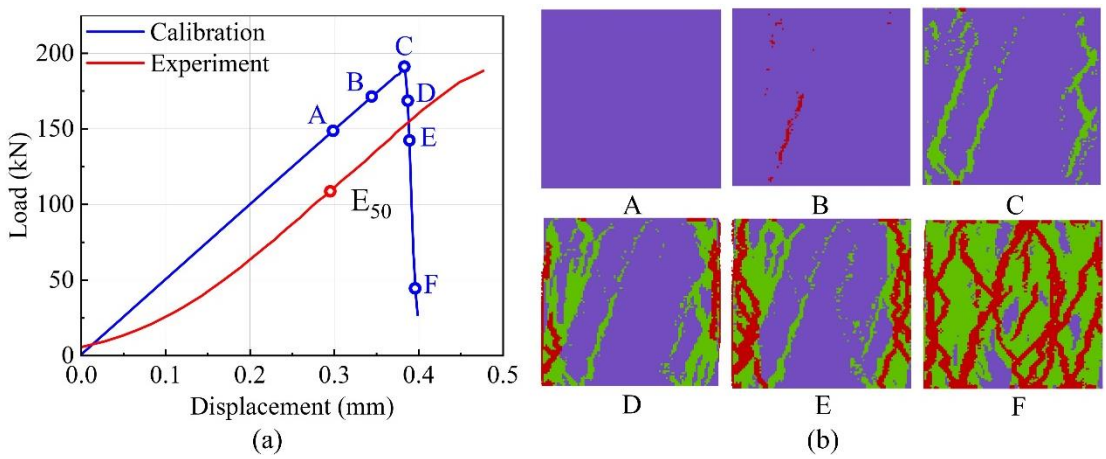

Fig. 5. Prediction results of red-sandstone: (a) uniaxial compressive strength curve; (b) rock fracturing process in six stages

Table 3. Numerical model parameters of red-sandstone

Parameters	Elastic modulus (GPa)	Poisson's ratio	Density (g/cm^3)	Tensile strength (MPa)	Cohesion (MPa)	Friction angle (°)
Red-sandstone	17	0.23	2.43	9	23	53

3.4 Calibration results

Table 4. Statistics of calibration results of numerical simulation parameters

Parameters	E (GPa)	Poisson's ratio	D (g/cm^3)	σ_t (MPa)	C (MPa)	Φ (°)	Strength (kN)	Error (%)
Granite	25	0.23	2.63	16	34	50	265.50	4.32
Marble	45	0.24	2.85	12	27	51	214.15	4.77
Red-sandstone	17	0.22	2.43	9	23	53	183.87	3.17

IV-1 Prediction results

4.1 Granite

4.1.1 Sample 1

According to the calibrated parameters, the uniaxial compressive strength curve of sample 1 is shown in Fig. 6(a). When the load value is 118.64 kN, the sample is damaged. The failure process of the sample is shown in Fig. 6(b), and the key points (A, B, C, D) have been marked on the curve.

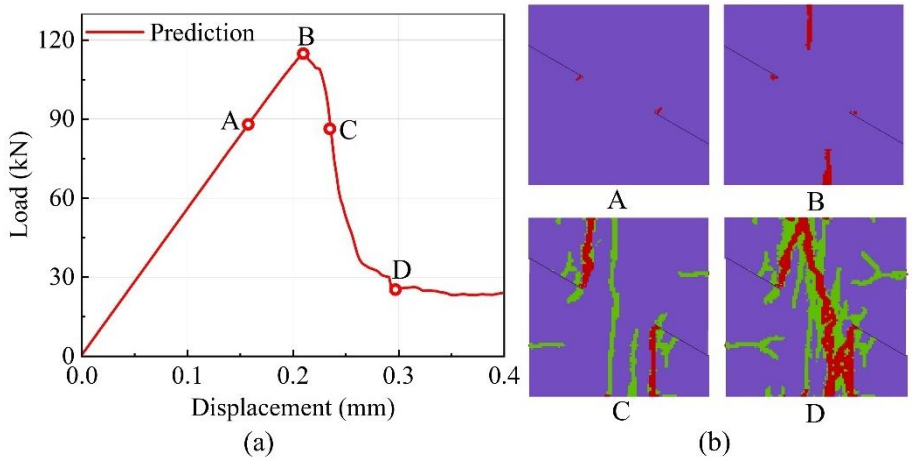

Fig. 6. Prediction results of sample 1: (a) uniaxial compressive strength curve; (b) rock fracturing process in four stages

4.1.2 Sample 2

According to the calibrated parameters, the uniaxial compressive strength curve of sample 2 is shown in Fig. 7(a). When the load value is 117.12 kN, the sample is damaged. The failure process of the sample is shown in Fig. 7(b), and the key points (A, B, C, D) have been marked on the curve.

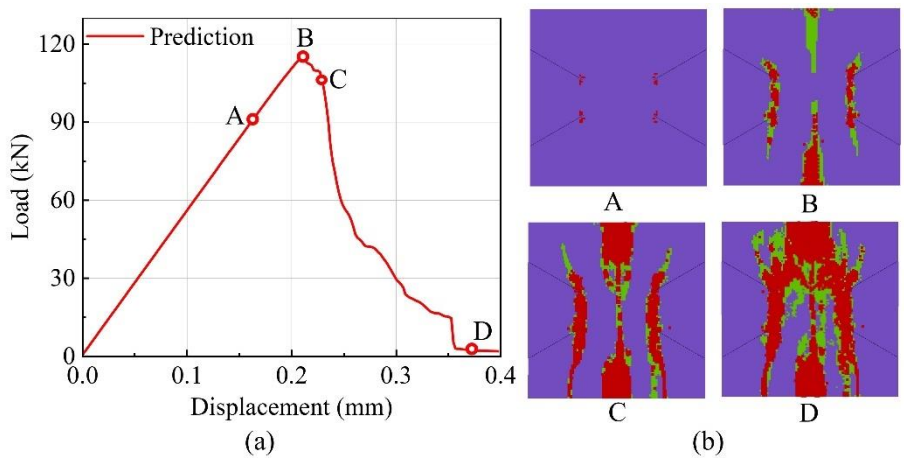

Fig. 7. Prediction results of sample 2: (a) uniaxial compressive strength curve; (b) rock fracturing process in four stages

4.1.3 Sample 3

According to the calibrated parameters, the uniaxial compressive strength curve of sample 3 is shown in Fig. 8(a). When the load value is 116.89 kN, the sample is damaged. The failure process of the sample is shown in Fig. 8(b), and the key points (A, B, C, D) have been marked on the curve.

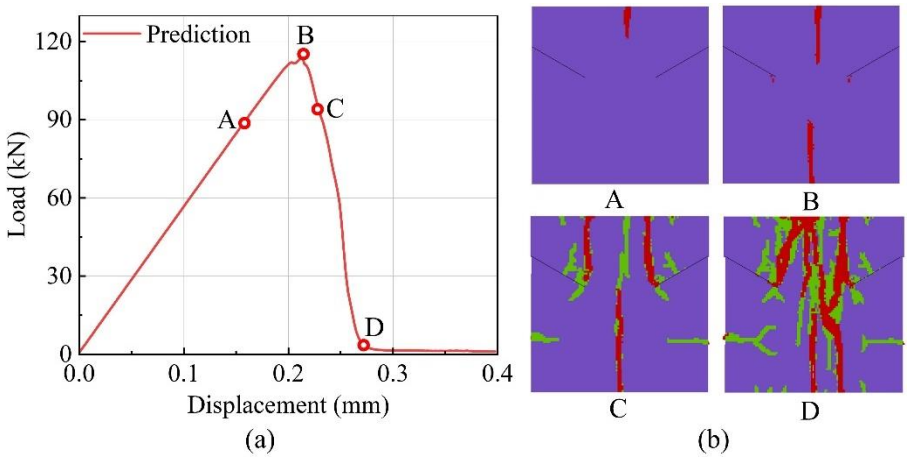

Fig. 8. Prediction results of sample 3: (a) uniaxial compressive strength curve; (b) rock fracturing process in four stages

4.1.4 Sample 4

According to the calibrated parameters, the uniaxial compressive strength curve of sample 4 is shown in Fig. 9(a). When the load value is 118.04 kN, the sample is damaged. The failure process of the sample is shown in Fig.9(b), and the key points (A, B, C, D) have been marked on the curve.

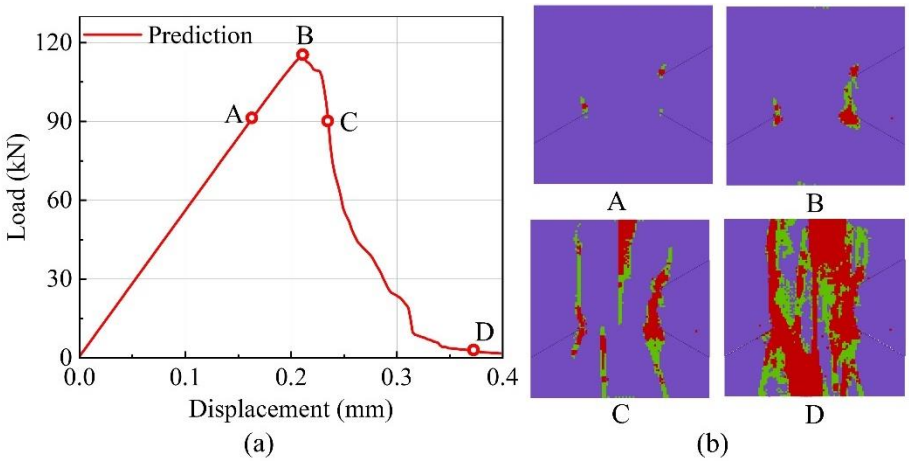

Fig. 9. Prediction results of sample 4: (a) uniaxial compressive strength curve; (b) rock fracturing process in four stages

4.2 Marble

4.2.1 Sample 1

According to the calibrated parameters, the uniaxial compressive strength curve of sample 1 is shown in Fig. 10(a). When the load value is 107.09 kN, the sample is damaged. The failure process of the sample is shown in Fig. 10(b), and the key points (A, B, C, D) have been marked on the curve.

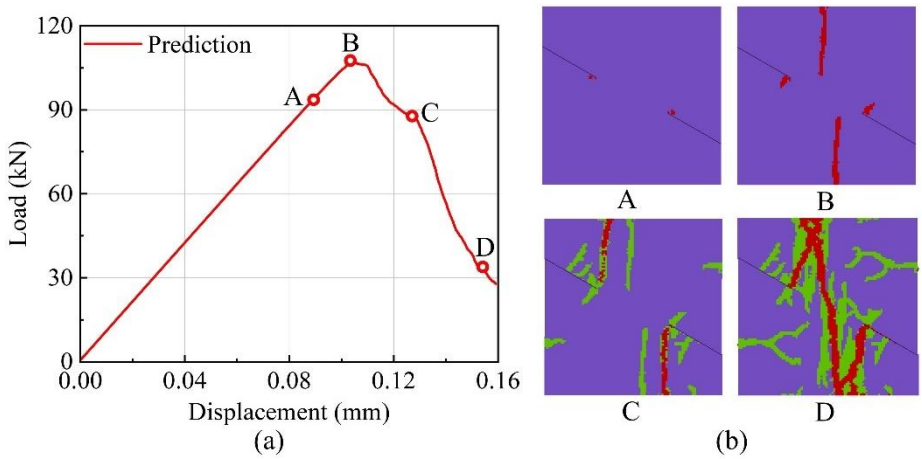

Fig. 10. Prediction results of sample 1: (a) uniaxial compressive strength curve; (b) rock fracturing process in four stages

4.2.2 Sample 2

According to the calibrated parameters, the uniaxial compressive strength curve of sample 2 is shown in Fig. 11(a). When the load value is 79.30 kN, the sample is damaged. The failure process of the sample is shown in Fig. 11(b), and the key points (A, B, C, D) have been marked on the curve.

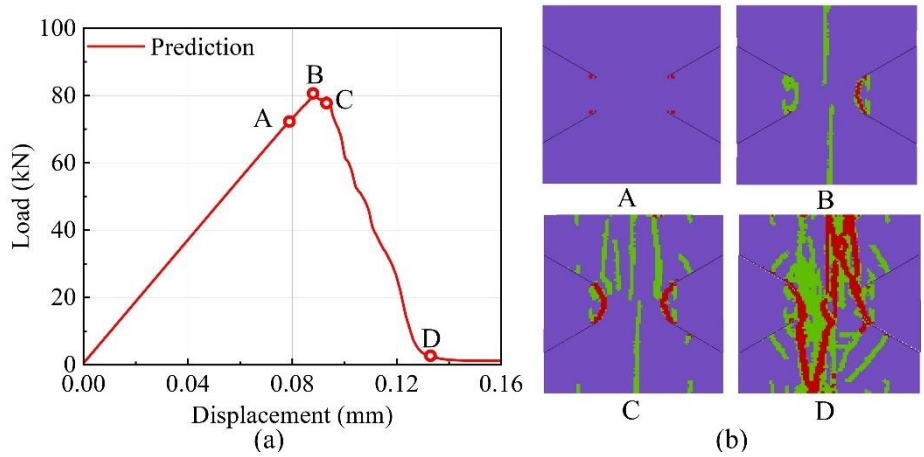

Fig. 11. Prediction results of sample 2: (a) uniaxial compressive strength curve; (b) rock fracturing process in four stages

4.2.3 Sample 3

According to the calibrated parameters, the uniaxial compressive strength curve of sample 3 is shown in Fig. 12(a). When the load value is 109.60 kN, the sample is damaged. The failure process of the sample is shown in Fig. 12(b), and the key points (A, B, C, D) have been marked on the curve.

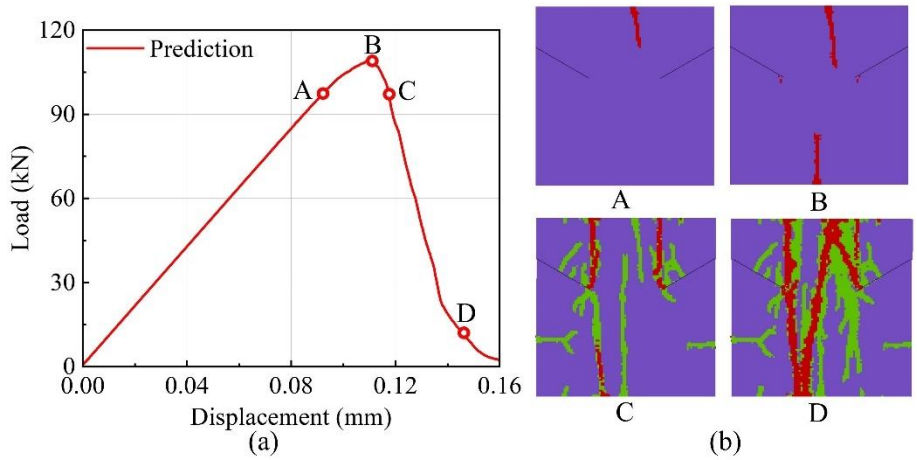

Fig. 12. Prediction results of sample 3: (a) uniaxial compressive strength curve; (b) rock fracturing process in four stages

4.2.4 Sample 4

According to the calibrated parameters, the uniaxial compressive strength curve of sample 4 is shown in Fig. 13(a). When the load value is 93.69 kN, the sample is damaged. The failure process of the sample is shown in Fig. 13(b), and the key points (A, B, C, D) have been marked on the curve.

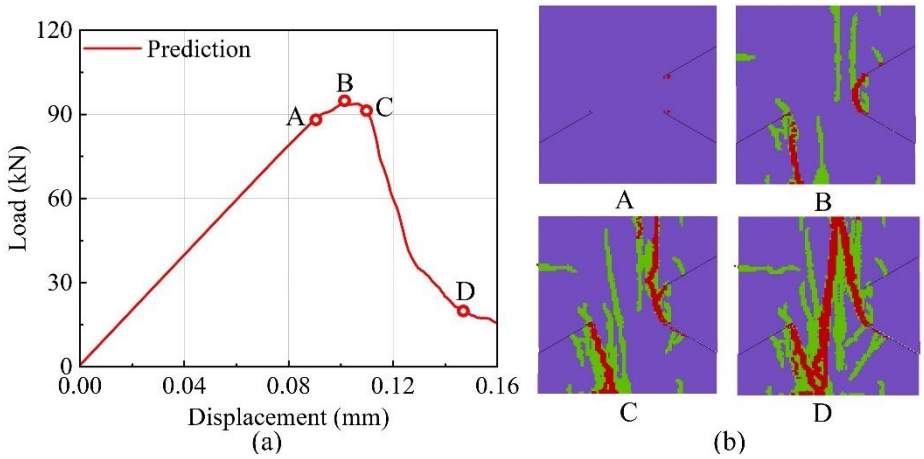

Fig. 13. Prediction results of sample 4: (a) uniaxial compressive strength curve; (b) rock fracturing process in four stages

4.3 Red-sandstone

4.3.1 Sample 1

According to the calibrated parameters, the uniaxial compressive strength curve of sample 1 is shown in Fig. 14(a). When the load value is 93.65 kN, the sample is damaged. The failure process of the sample is shown in Fig. 14(b), and the key points (A, B, C, D) have been marked on the curve.

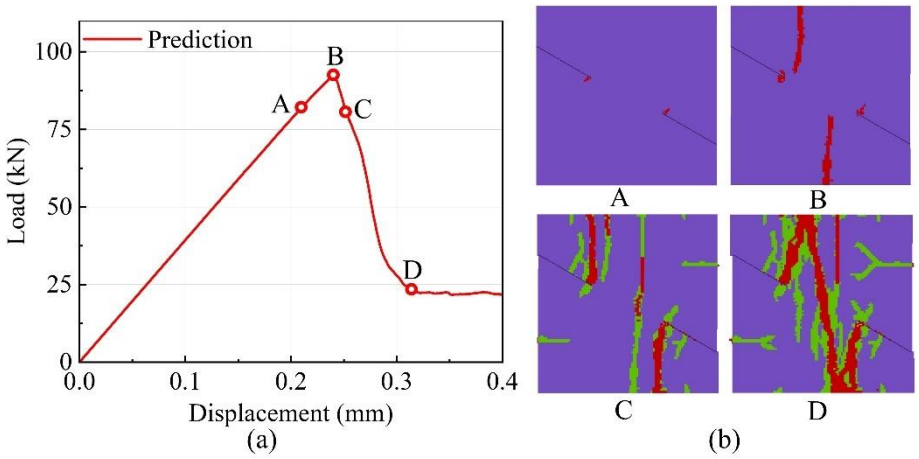

Fig. 14. Prediction results of sample 1: (a) uniaxial compressive strength curve; (b) rock fracturing process in four stages

4.3.2 Sample 2

According to the calibrated parameters, the uniaxial compressive strength curve of sample 2 is shown in Fig. 15(a). When the load value is 68.95 kN, the sample is damaged. The failure process of the sample is shown in Fig. 15(b), and the key points (A, B, C, D) have been marked on the curve.

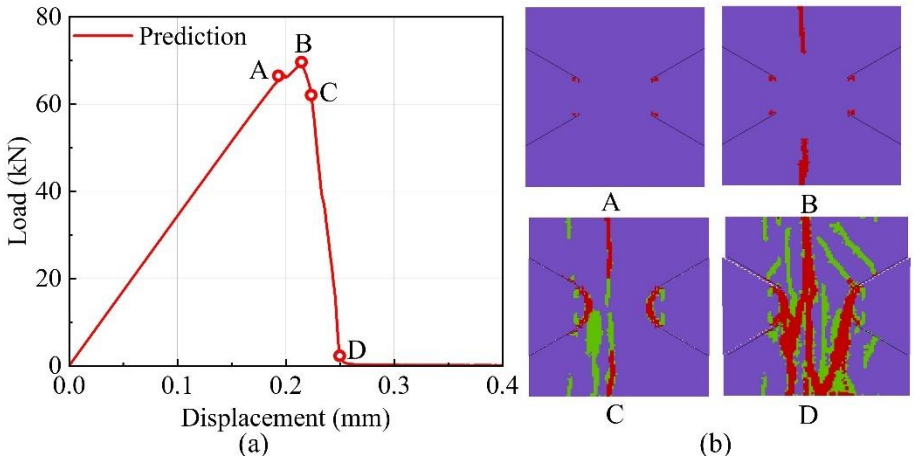

Fig. 15. Prediction results of sample 2: (a) uniaxial compressive strength curve; (b) rock fracturing process in four stages

4.3.3 Sample 3

According to the calibrated parameters, the uniaxial compressive strength curve of sample 3 is shown in Fig. 16(a). When the load value is 98.15 kN, the sample is damaged. The failure process of the sample is shown in Fig. 16(b), and the key points (A, B, C, D) have been marked on the curve.

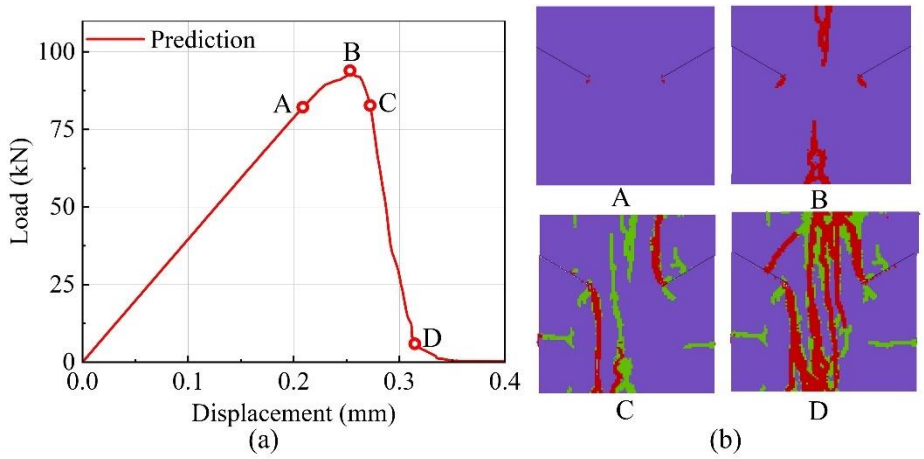

Fig. 16. Prediction results of sample 3: (a) uniaxial compressive strength curve; (b) rock fracturing process in four stages

4.3.4 Sample 4

According to the calibrated parameters, the uniaxial compressive strength curve of sample 4 is shown in Fig. 17(a). When the load value is 77.82 kN, the sample is damaged. The failure process of the sample is shown in Fig. 17(b), and the key points (A, B, C, D) have been marked on the curve.

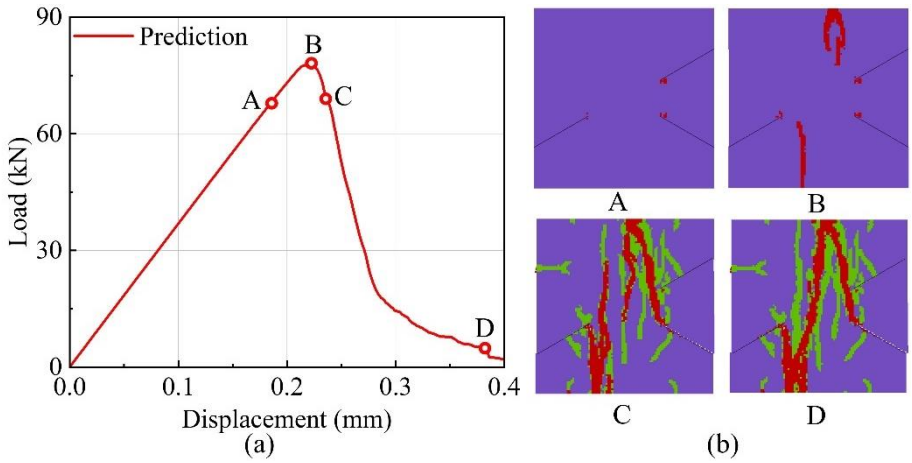

Fig. 17. Prediction results of sample 4: (a) uniaxial compressive strength curve; (b) rock fracturing process in four stages

4.4 Prediction results

Table 5. Statistics of prediction results for three types of rocks.

Lithologies	Peak compressive load(kN)			
	Sample1	Sample2	Sample3	Sample4
Granite	118.64	117.12	116.89	118.04
Marble	107.09	79.30	109.60	93.69
Red-sandstone	93.65	68.95	98.15	77.82

Stage II

II-2 Numerical modelling

Similar to the complete rock samples, the dimensions of numerical model of prefabricated cracked rock samples are 50 mm × 50 mm × 30 mm and the particle size is 1 mm. The total number of particles is 75000. The upper and lower boundaries of the model are wall boundaries. A uniform downward force of F_y is applied on the upper part of the model with a speed of 1 mm/min until the model is damaged (as shown in Fig. 18). The model adopts multi-body failure criterion and adaptive damping. The rock mass is assumed to be isotropic and homogeneous.

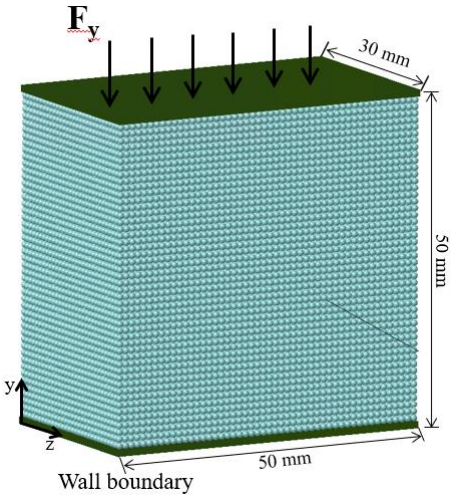

Fig. 18. Numerical model.

III-2 Calibration results

3.1 Granite (sample 1)

As shown in Fig. 19(a), the red curve is the experimental result and the blue curve is the numerical simulation result after parameter calibration. Four characteristic points (A, B, C, and D) of the curve are selected to describe the failure process of the sample. It can be found from the figure that the uniaxial compressive strength of the model is 207.57 kN and the experimental result is 202.67 kN, with a difference of 2.37%. The failure process of the model is shown in Fig. 19(b). The calibration results of granite parameters are shown in Table 6.

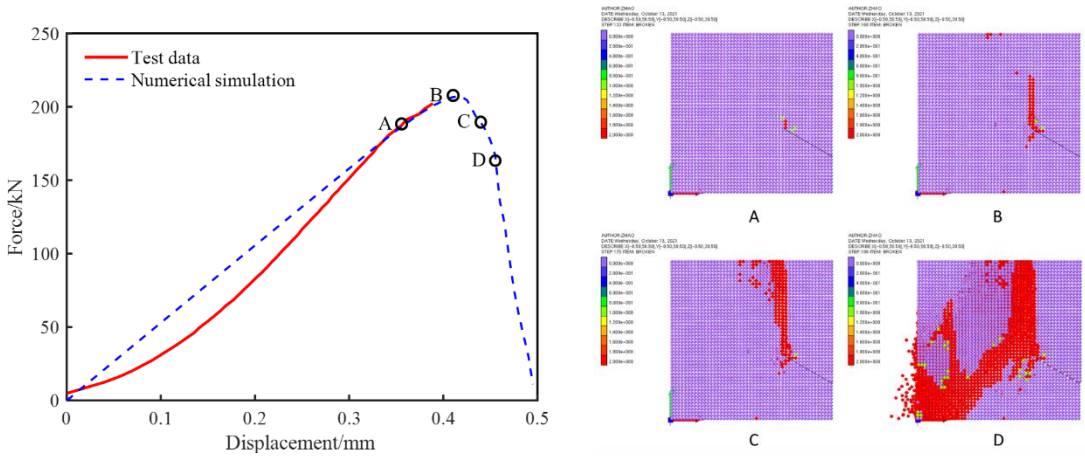

(a) (b)

Fig. 19. Numerical simulation of uniaxial compressive strength test of granite: (a) uniaxial compressive strength curve; (b) rock fracturing process in four stages

Table 6. Calibrated parameters for granite samples

Parameters	Elastic modulus (GPa)	Poisson's ratio	Density (g/cm^3)	Tensile strength (MPa)	Cohesion (MPa)	Friction angle (°)
Granite	18.5	0.15	2.63	25	32	56

3.2 Marble (sample 1)

As shown in Fig. 20(a), the red curve is the experimental result and the blue curve is the numerical simulation result after parameter calibration. Four characteristic points (A, B, C, and D) of the curve are selected to describe the failure process of the sample. It can be found from the figure that the uniaxial compressive strength of the model is 160.28 kN and the experimental result is 168.80 kN, with a difference of 5.32%. The failure process of the model is shown in Fig. 20(b). The calibration results of granite parameters are shown in Table 7.

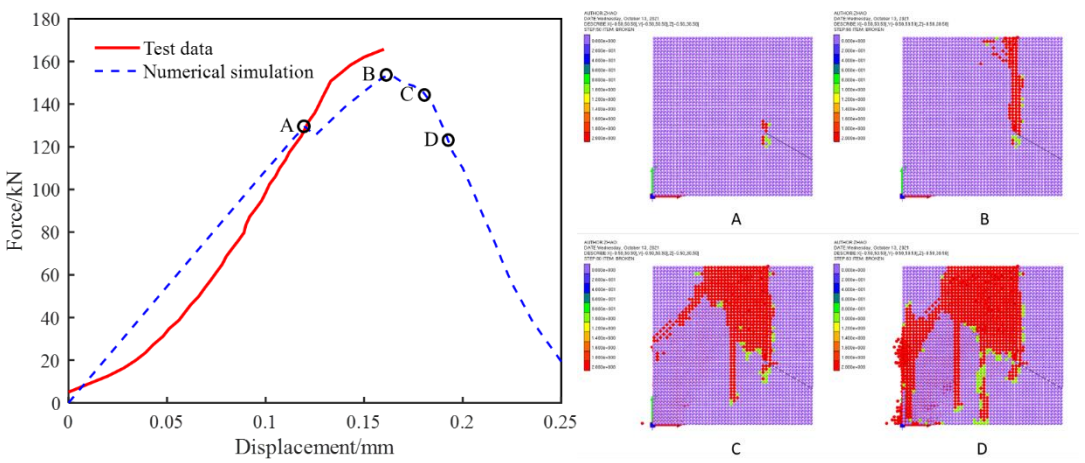

(a) (b)

Fig. 20. Uniaxial compressive strength curve of marble: (a) uniaxial compressive strength curve; (b) rock fracturing process in four stages

Table 7. Numerical model parameters of marble

Parameters	Elastic modulus (GPa)	Poisson's ratio	Density (g/cm^3)	Tensile strength (MPa)	Cohesion (MPa)	Friction angle (°)
Marble	40	0.2	2.85	25	28	55

3.3 Red-sandstone (sample 1)

As shown in Fig. 21(a), the red curve is the experimental result and the blue curve is the numerical simulation result after parameter calibration. Four characteristic points (A, B, C, and D) of the curve are selected to describe the failure process of the sample. It can be found from the figure that the uniaxial compressive strength of the model is 131.28 kN and the experimental result is 133.62 kN, with a difference of 1.78%. The failure process of the model is shown in Fig. 21(b). The calibration results of granite parameters are shown in Table 8.

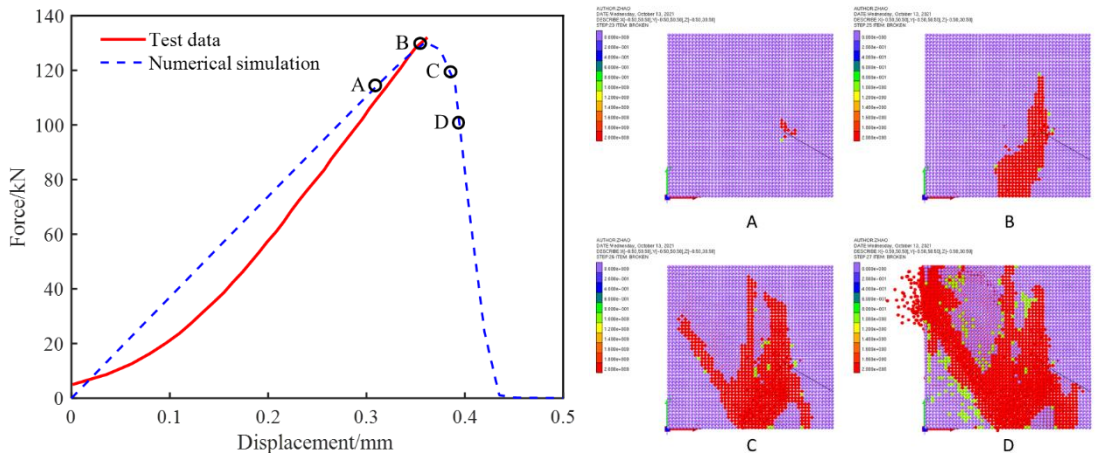

(a) (b)

Fig. 21. Failure process of red-sandstone: (a) uniaxial compressive strength curve; (b) rock fracturing process in four stages

Table 8. Numerical model parameters of red-sandstone

Parameters	Elastic modulus (GPa)	Poisson's ratio	Density (g/cm^3)	Tensile strength (MPa)	Cohesion (MPa)	Friction angle (°)
Red-sandstone	13	0.23	2.42	15	22	53

3.4 Calibration results

Table 9. Statistics of calibration results of numerical simulation parameters

Parameters	E (GPa)	Poisson's ratio	D (g/cm)	σ_t (MPa)	C (MPa)	Φ (°)	Strength (kN)	Error (%)
Granite	18.5	0.15	2.63	25	32	56	207.57	2.37
Marble	40	0.2	2.85	25	28	55	160.28	5.32
Red-sandstone	13	0.23	2.42	15	22	53	131.28	1.78

IV-2 Prediction results

4.1 Granite

4.1.1 Sample 1

According to the calibrated parameters, the uniaxial compressive strength curve of sample 1 is shown in Fig. 22(a). When the load value is 140.98 kN, the sample is damaged. The failure process of the sample is shown in Fig. 22(b), and the key points (A, B, C, D) have been marked on the curve.

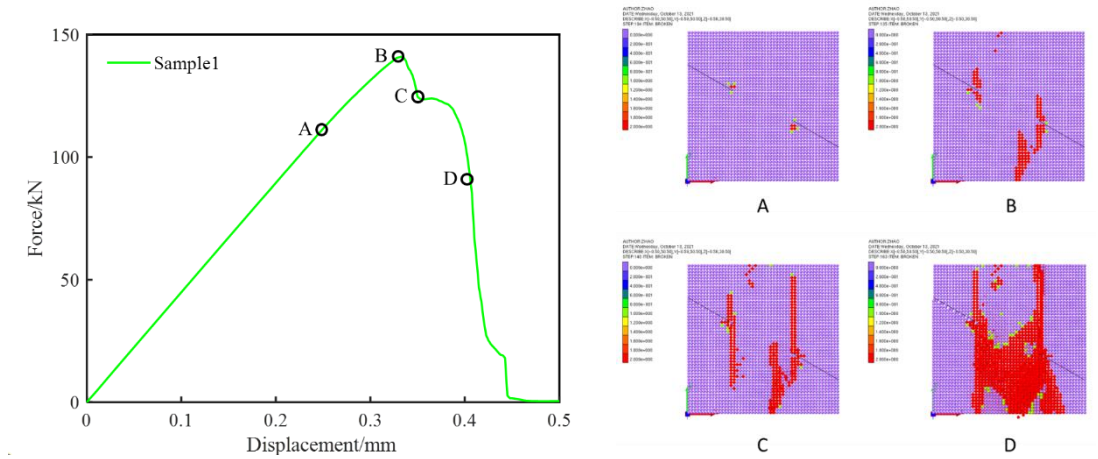

(a) (b)

Fig. 22. Prediction results of sample 1: (a) uniaxial compressive strength curve; (b) rock fracturing process in four stages

4.1.2 Sample 2

According to the calibrated parameters, the uniaxial compressive strength curve of sample 2 is shown in Fig. 23(a). When the load value is 106.58 kN, the sample is damaged. The failure process of the sample is shown in Fig. 23(b), and the key points (A, B, C, D) have been marked on the curve.

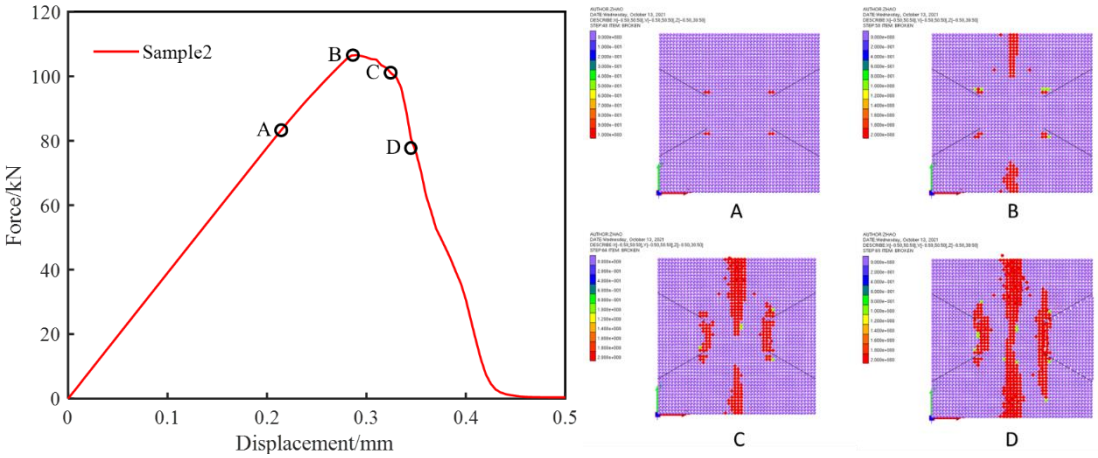

(a) (b)

Fig. 23. Prediction results of sample 2: (a) uniaxial compressive strength curve; (b) rock fracturing process in four stages

4.1.3 Sample 3

According to the calibrated parameters, the uniaxial compressive strength curve of sample 3 is

shown in Fig. 24(a). When the load value is 134.55 kN, the sample is damaged. The failure process of the sample is shown in Fig.24(b), and the key points (A, B, C, D) have been marked on the curve.

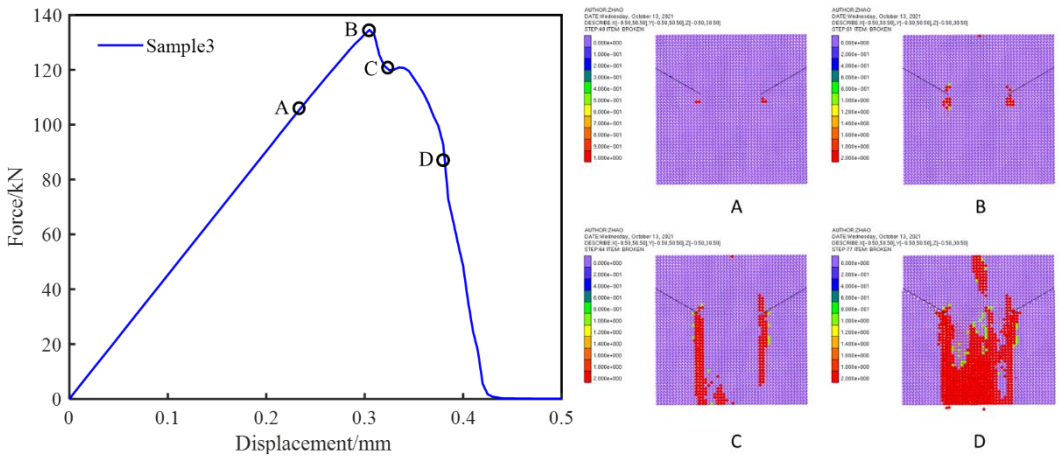

(a) (b)

Fig. 24. Prediction results of sample 3: (a) uniaxial compressive strength curve; (b) rock fracturing process in four stages

4.1.4 Sample 4

According to the calibrated parameters, the uniaxial compressive strength curve of sample 4 is shown in Fig. 25(a). When the load value is 125.46 kN, the sample is damaged. The failure process of the sample is shown in Fig. 25(b), and the key points (A, B, C, D) have been marked on the curve.

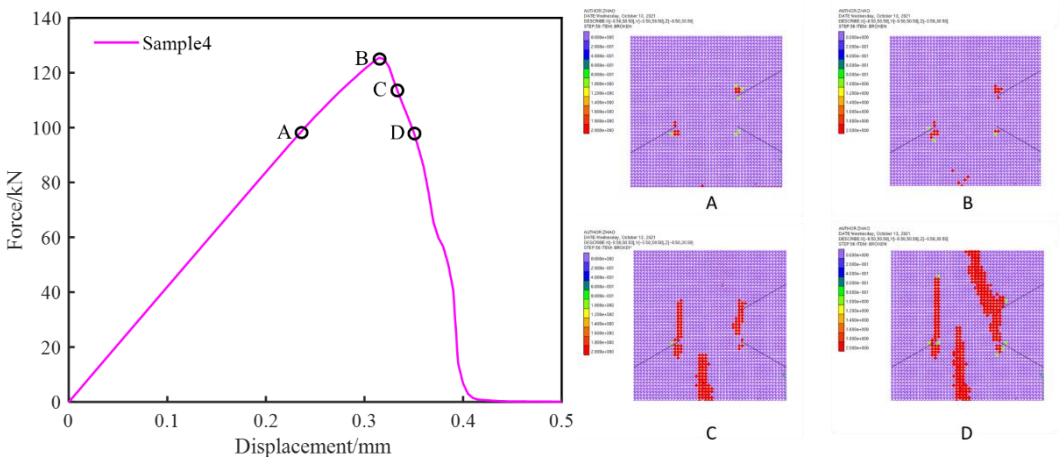

(a) (b)

Fig. 25. Prediction results of sample 4: (a) uniaxial compressive strength curve; (b) rock fracturing process in four stages

4.2 Marble

4.2.1 Sample 1

According to the calibrated parameters, the uniaxial compressive strength curve of sample 1 is shown in Fig. 26(a). When the load value is 94.63 kN, the sample is damaged. The failure process of the sample is shown in Fig. 26(b), and the key points (A, B, C, D) have been marked on the

curve.

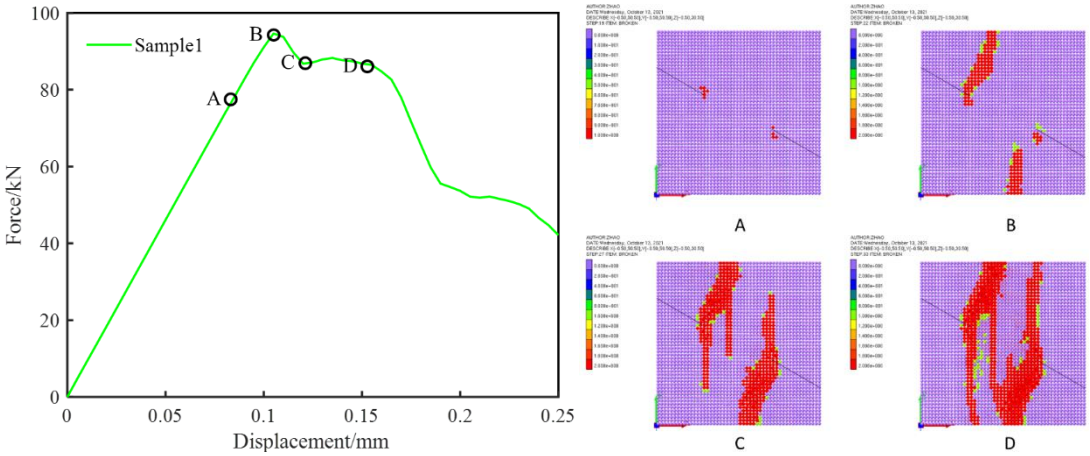

(a) (b)

Fig. 26. Prediction results of sample 1: (a) uniaxial compressive strength curve; (b) rock fracturing process in four stages

4.2.2 Sample 2

According to the calibrated parameters, the uniaxial compressive strength curve of sample 2 is shown in Fig. 27(a). When the load value is 88.13 kN, the sample is damaged. The failure process of the sample is shown in Fig. 27(b), and the key points (A, B, C, D) have been marked on the curve.

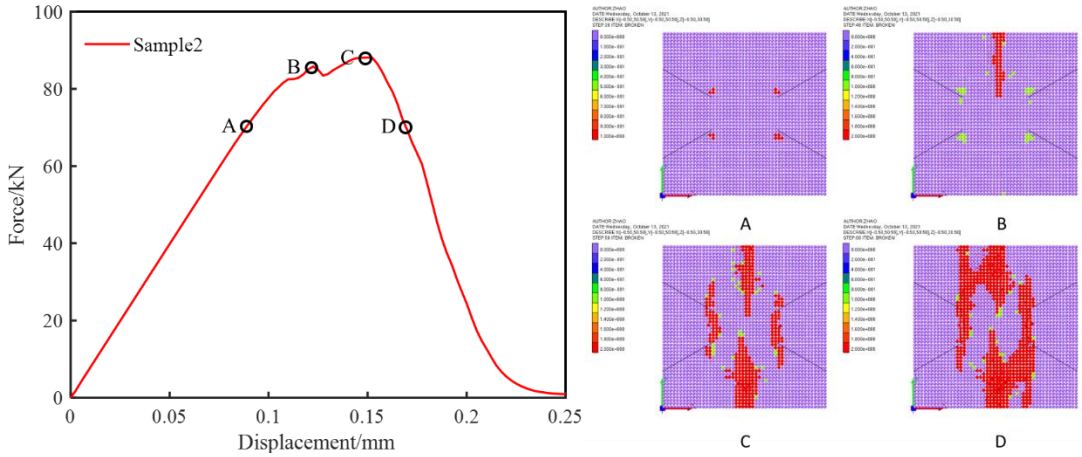

(a) (b)

Fig. 27. Prediction results of sample 2: (a) uniaxial compressive strength curve; (b) rock fracturing process in four stages

4.2.3 Sample 3

According to the calibrated parameters, the uniaxial compressive strength curve of sample 3 is shown in Fig. 28(a). When the load value is 106.37 kN, the sample is damaged. The failure process of the sample is shown in Fig. 28(b), and the key points (A, B, C, D) have been marked on the curve.

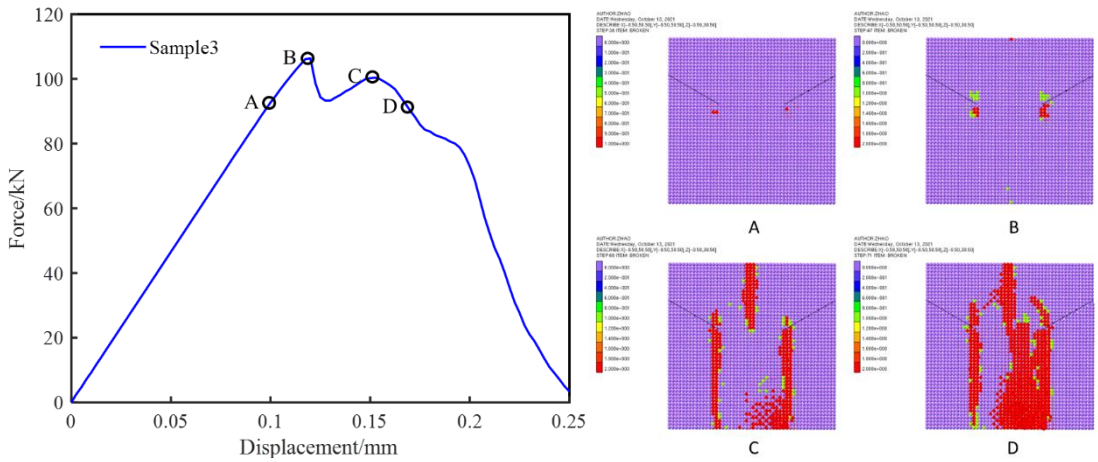

(a) (b)

Fig. 28. Prediction results of sample 3: (a) uniaxial compressive strength curve; (b) rock fracturing process in four stages

4.2.4 Sample 4

According to the calibrated parameters, the uniaxial compressive strength curve of sample 4 is shown in Fig. 29(a). When the load value is 98.47 kN, the sample is damaged. The failure process of the sample is shown in Fig. 29(b), and the key points (A, B, C, D) have been marked on the curve.

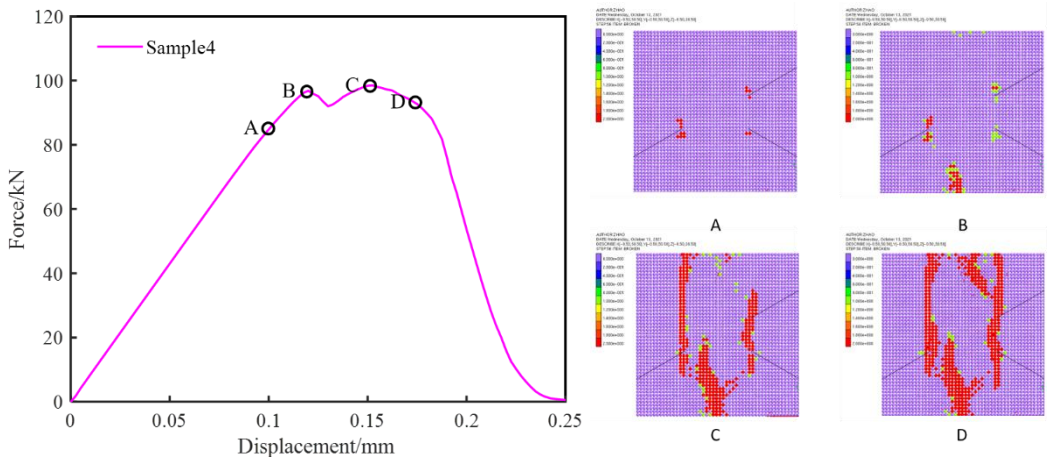

(a) (b)

Fig. 29. Prediction results of sample 4: (a) uniaxial compressive strength curve; (b) rock fracturing process in four stages

4.3 Red-sandstone

4.3.1 Sample 1

According to the calibrated parameters, the uniaxial compressive strength curve of sample 1 is shown in Fig. 30(a). When the load value is 101.26 kN, the sample is damaged. The failure process of the sample is shown in Fig. 30(b), and the key points (A, B, C, D) have been marked on the curve.

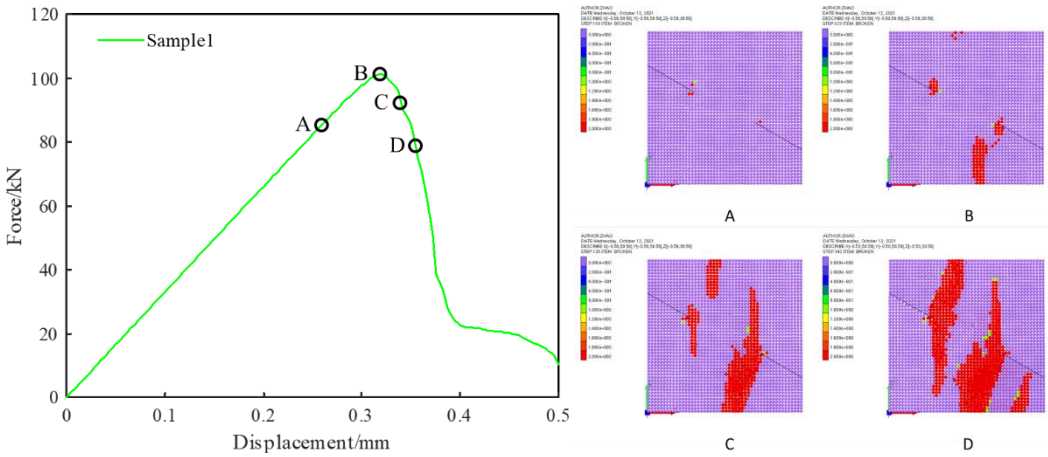

(a) (b)

Fig. 30. Prediction results of sample 1: (a) uniaxial compressive strength curve; (b) rock fracturing process in four stages

4.3.2 Sample 2

According to the calibrated parameters, the uniaxial compressive strength curve of sample 2 is shown in Fig. 31(a). When the load value is 78.28 kN, the sample is damaged. The failure process of the sample is shown in Fig. 31(b), and the key points (A, B, C, D) have been marked on the curve.

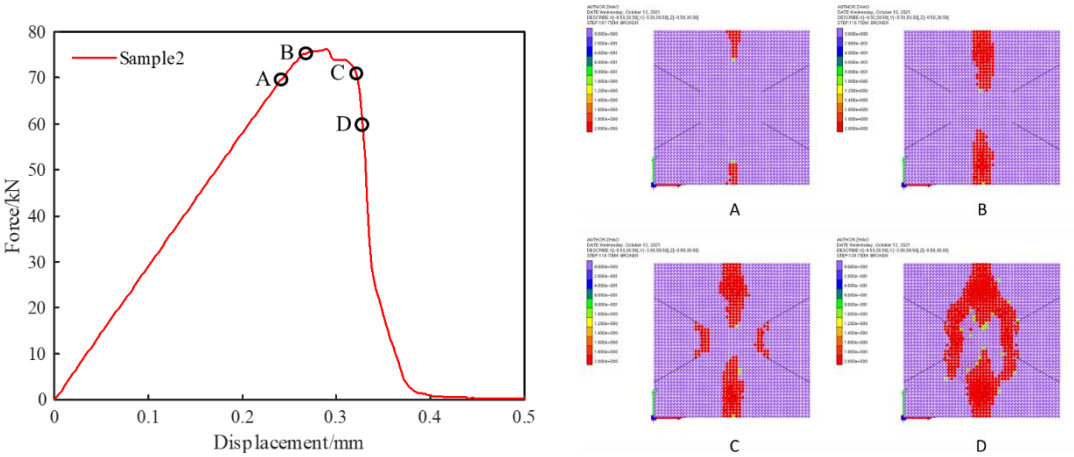

(a) (b)

Fig. 31. Prediction results of sample 2: (a) uniaxial compressive strength curve; (b) rock fracturing process in four stages

4.3.3 Sample 3

According to the calibrated parameters, the uniaxial compressive strength curve of sample 3 is shown in Fig. 32(a). When the load value is 100.13 kN, the sample is damaged. The failure process of the sample is shown in Fig. 32(b), and the key points (A, B, C, D) have been marked on the curve.

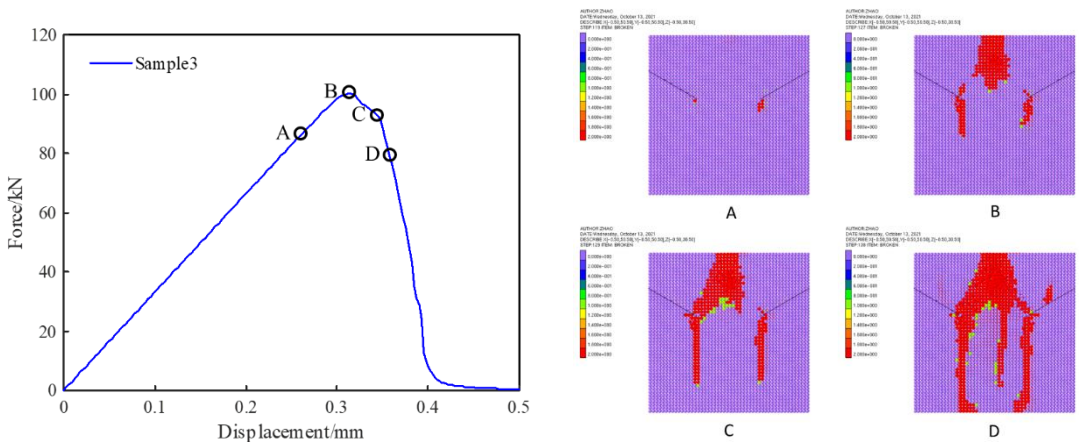

(a) (b)

Fig. 32. Prediction results of sample 3: (a) uniaxial compressive strength curve; (b) rock fracturing process in four stages

4.3.4 Sample 4

According to the calibrated parameters, the uniaxial compressive strength curve of sample 4 is shown in Fig. 33(a). When the load value is 87.58 kN, the sample is damaged. The failure process of the sample is shown in Fig. 33(b), and the key points (A, B, C, D) have been marked on the curve.

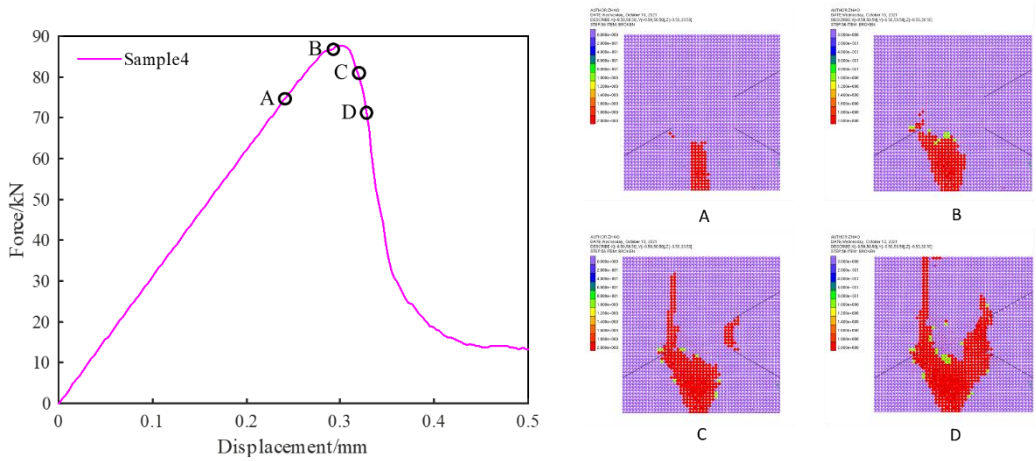

(a) (b)

Fig. 33. Prediction results of sample 4: (a) uniaxial compressive strength curve; (b) rock fracturing process in four stages

4.4 Prediction results

Table 10. Statistics of prediction results for three types of rocks.

Lithologies	Peak compressive load(kN)			
	Sample1	Sample2	Sample3	Sample4
Granite	140.98	106.58	134.55	125.46
Marble	94.63	88.13	106.37	98.47
Red-sandstone	101.26	78.28	100.13	87.58

V Conclusions

In this report, the parameters of numerical model are calibrated according to the experimental results of uniaxial compression of three rock samples. The error of uniaxial compression strength between the numerical and experimental results is almost less than 5%. The fracture patterns are almost the same as the experimental results. Therefore, it can be considered that the result of the calibration parameters is correct. In addition, according to the results of calibration parameters, the fracture patterns of other samples are predicted. We conclude that 4D-LSM is a powerful tool for studying the mechanical behavior, strength and failure of rocks.

Acknowledgment

Thank Professor Gao-Feng Zhao for his guidance of this competition.

References

[1] Zhao, G.-F. Developing a four-dimensional lattice spring model for mechanical responses of solids. Computer Methods in Applied Mechanics and Engineering. 2017, 315: 881-895.

[2] Hu, X.-D., Zhao, G.-F., Deng, X.-F., Hao, Y.-F., Fan, L.-F., Ma, G.-W., Zhao, J. Application of the four-dimensional lattice spring model for blasting wave propagation around the underground rock cavern. Tunnelling and Underground Space Technology. 2018, 82: 135-147.